


Pinning effects in a two-dimensional cluster glassWenlong Wang^{1,2,*}, Rogelio Díaz-Méndez², Mats Wallin², Jack Lidmar² and Egor Babaev²¹College of Physics, Sichuan University, Chengdu 610065, China²Department of Physics, Royal Institute of Technology, Stockholm, SE-106 91, Sweden (Received 14 November 2020; revised 3 October 2021; accepted 4 October 2021; published 26 October 2021)

We study numerically the nonequilibrium glass formation and depinning transition of a system of two-dimensional cluster-forming monodisperse particles in the presence of pinning disorder. The pairwise interaction potential is nonmonotonic and is motivated by the intervortex forces in type-1.5 superconductors but also applies to a variety of other systems. Such systems can form cluster glasses due to the intervortex interactions following a thermal quench, without underlying disorder. We study the effects of vortex pinning in these systems. We find that a small density of pinning centers of moderate depth has a limited effect on vortex glass formation, i.e., formation of vortex glasses is dominated by intervortex interactions. At higher densities, pinning can significantly affect glass formation. The cluster glass depinning, under a constant driving force, is found to be plastic, with features distinct from non-cluster-forming systems such as clusters merging and breaking. We find that, in general, vortices with cluster-forming interaction forces can exhibit stronger pinning effects than regular vortices.

DOI: [10.1103/PhysRevB.104.144206](https://doi.org/10.1103/PhysRevB.104.144206)**I. INTRODUCTION**

In the past few decades, there have been significant ongoing efforts directed to understanding the rich properties of vortex matter in type-2 superconductors [1]. The glass formation has been intensively studied for vortex systems with pinning disorder [1–4]. One major research theme is investigating the effects of pinning disorder on vortex glass formation and the corresponding depinning transition and dynamics upon driving. This is important in superconductor applications, as dissipationless current-carrying states require arresting the dynamics of vortices. In the much less studied multicomponent superconductors, the vortex interactions can take complex forms as a result of multiple competing (attractive and repulsive) interaction length scales for vortices that are thermodynamically stable in large ranges of fields and temperatures [5–9]. This has been proposed not only in superconductors with several superconducting components but also in multilayer systems with different coherence (ξ_i) and penetration (λ_i) lengths [10–12]. In the bulk of intrinsic type-1.5 superconductors, intervortex forces are long-range attractive and short-range repulsive [5,6,8,9].

The origin of nonmonotonic vortex interactions is the existence of multiple coherence lengths related to either multiple broken symmetries [13,14] or multiple bands with weak or frustrated interband coupling [8]. This arises because the core-core interaction is attractive over the length scale set by the coherence length. In the multicomponent case, a vortex core has a composite matreshka structure with multiple length scales. The repulsive interaction originates from current-

current and magnetic interaction and has the scale of magnetic field penetration length. However, multiple magnetic modes giving rise to multiple repulsive length scales are also possible [15,16]. For thin films, an additional repulsive interaction arises due to the magnetic stray fields [17]. Similarly, in layered systems multiple repulsive length scales originate from the disparity of magnetic field penetration lengths in different layers [11]. The layered systems allow for preparing desired intervortex interaction potentials by controlling materials and thickness.

Various multiband materials have been proposed to fall into the type-1.5 class [18–20]. In double-transition materials, type-1.5 behavior is almost generic due to the diverging coherence length at the lower transition [13,14]. Many vortex phases have been predicted for type-1.5 superconducting systems [11,12,21,22]. However, this type of ordering is much more general. The cluster and stripe phases are in many ways similar to ones emerging in a wide range of cluster-forming monodisperse particle systems such as colloidal suspensions and ultracold atoms [23–32], soft matter [33], and also electron liquids in quantum Hall systems [34–38].

In type-2 non-cluster-forming vortex systems, glass phases are associated with pinning while, in contrast, with cluster-forming interactions the situation is different and quench dynamics can produce a glass also without pinning [12]. For this class of interactions, particle systems undergo a crystal-to-glass transition [12,25], in which a glassy phase establishes sharply around a particular value of the degree of frustration of the material. Glass formation in the absence of disorder is known to occur for polydisperse systems [33]. The crystal-to-glass transition differs from the well-known liquid-to-glass (or glass-forming-liquid) transition in both qualitative and quantitative ways. In the case of cluster-forming systems,

*wenlongcmp@scu.edu.cn

quenches from a disordered configuration to a temperature below the hopping activation of single vortices spontaneously generate an effective polydispersity in the form of clusters with different sizes that form cluster glass states [12].

A central assumption that we make here, which is supported by the simulations [12], is that there is a separation of time scales such that there is a metastable regime of interest here for the times observed in the simulations where clusters formed in a rapid quench are stable, while the time scale for relaxation towards equilibrium is much longer and is not further considered here.

For many glass-forming systems, analysis of the nature of underlying equilibrium states can be highly nontrivial, typically involving extensive studies of relaxation dynamics. However, for cluster glasses formed by a rapid quench, the situation is different [12,25]. In the pure case without pinning, the underlying equilibrium state is typically an ordered cluster crystal with uniform cluster size produced by slow cooling of a liquid state. In this sense, the equilibrium states will not directly connect to the properties of nonequilibrium cluster glass states with nonuniform cluster size that are of interest in this paper. The problem we study and its possible experimental realization also motivates new open questions such as the connections to the melting and shear flows of disordered clusters in similar soft matter systems [32,39–41].

The effect of pinning is much less understood for type-1.5 superconductors than in non-cluster-forming vortex systems. The especially interesting question is the effect of pinning on vortex cluster glass formation. In addition, the nonequilibrium depinning transition of monodisperse particles has been intensively studied for particle solids; see Ref. [28] for a recent review. However, the depinning of pattern-forming systems, in particular, the cluster phases [42], which are experimentally relevant, have not been extensively studied. Indeed, even the nature of depinning and the main features of the flowing phase have not been explored in detail.

The main purpose of this paper is to present a study of cluster glass formation following a thermal quench in presence of pinning disorder and the corresponding depinning dynamics when a constant external force is applied. We are interested in, e.g., how pinning disorder density and depth affect glass formation, and in fact whether cluster glass itself remains well defined, and for depinning we are interested in the nature of the depinning transition, i.e., elastic depinning or plastic depinning, and the main features of the flowing phase. Here, plastic flow refers to the flowing clusters changing their neighbors, while in elastic flow they do not.

For traps of a moderate depth, we find that cluster glass remains reasonably well defined and persists even to the regime of dense pinning. The depinning transition is found to be plastic and the flowing phase has a number of interesting features compared with the non-cluster-forming counterpart. In addition to the cluster plastic flow, the clusters can undergo structural transformations. Most notably, the clusters can merge or break up due to thermal effects and, more importantly, the interplay between the pinning force and the driving force. The effective polydispersity assists the plastic flow also in that a smaller cluster tends to have a better mobility and, consequently, diffuses and escapes from a trap faster. Finally,

we have compared the depinning of a cluster glass and a particle glass, finding that the cluster glass exhibits stronger pinning effects. This suggests that cluster vortex glasses might be suitable for certain technological applications where a high critical current is desired.

The paper is organized as follows: The model, observables, and numerical methods are described in Sec. II. Numerical results are given in Sec. III. Finally, a summary and discussion of the main findings is presented in Sec. IV.

II. MODEL, OBSERVABLES, AND METHODS

A. Model

We study a system of two-dimensional monodisperse particles interacting via an effective pairwise potential, and with pinning centers, and an external driving force modeled by the following dimensionless Hamiltonian:

$$H = \sum_{i<j} U_{ij} - \sum_{i\alpha} U_p \exp[-r_{i\alpha}^2/(2\sigma^2)] - F_D \sum_i x_i. \quad (1)$$

The indices i, j run from 1 to the number of particles N , and α runs from 1 to the number of pinning centers M . The particles are placed on an $L \times L$ square with coordinates $\{x_i, y_i\}$ under periodic boundary conditions. The three terms are for particle-particle interactions, randomly located and quenched Gaussian pinning centers, and a constant driving force along the x direction, respectively. The density of particles is $n = N/L^2$ and the density of impurities is $m = M/L^2 = nM/N$. $U_p > 0$ and σ denote the depth and size of the pinning centers, respectively. F_D denotes the strength of the driving force, which for vortices in a superconductor the Lorentz force on a vortex is $F_D = j\phi_0$, where j is the sheet current density, ϕ_0 is the flux quantum, and the force is perpendicular to the applied current. We used $\sigma = 0.7$ unless specified otherwise, which is approximately half of the lattice constant of the corresponding cluster crystal in the absence of disorder and driving. A point-particle representation is applicable for superconducting vortices where the interparticle interaction forces are chosen to be consistent with those obtained in superconductivity models.

The potential, relevant to vortex interactions in type-1.5 superconductors, is defined as

$$U(r) = \begin{cases} U_0 - C_0(r + 0.15)^4, & \text{if } r \leq 0.15 \\ \sum_{l=1}^3 C_l K_0(r/\alpha_l), & \text{if } r > 0.15, \end{cases} \quad (2)$$

where K_0 is the modified Bessel function of the second kind and the parameters are $U_0 = 2.6796$, $C_0 = 144.3760$, $C_1 = 37.2100$, $\alpha_1 = 0.1405$, $C_2 = -36.1911$, $\alpha_2 = 0.1960$, $C_3 = 7.2900$, and $\alpha_3 = 0.4200$. The potential is plotted as the red curve in Fig. 1. It is similar to the one used in Ref. [12] in medium and long ranges, but it features an attractive intermediate part and the unphysical divergence from long-range asymptotic analysis at the origin is regularized with a fourth-order polynomial to match better with the full numerically calculated potential [10].

For comparison, we also use the standard repulsive type-2 vortex interaction potential from a single modified Bessel function $U(r) = CK_0(r/\alpha)$ with parameters $C = 1.7511$ and

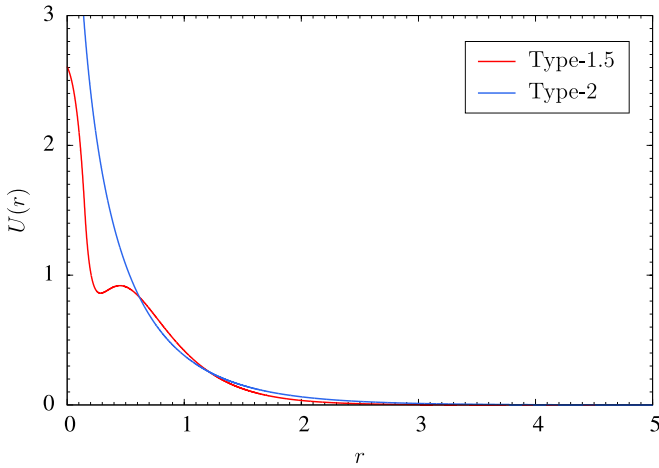


FIG. 1. Pairwise particle-particle, i.e., vortex-vortex interaction potentials. The red curve is a cluster-forming potential [Eq. (2)] while the blue curve forms single-particle crystals. They model vortex interactions in type-1.5 and type-2 superconductors, respectively.

$\alpha = 0.6726$, shown as the blue curve in Fig. 1. This potential generates single-particle crystals with no clustering behavior.

The physical origin of the potential Eq. (2) is the following. In the type-1.5 regime, a superconductor has several coherence lengths, originating from the individual superconducting components. Some of the coherence lengths are larger and some are smaller than the magnetic field penetration length. The resulting intervortex forces asymptotically have the form of a sum of Bessel functions which give contributions to attractive interactions at the coherence length scales and repulsive interaction at the magnetic field penetration length [5–7,9,14]. In the standard type-1.5 regime, the intervortex interaction is short-range repulsive and long-range attractive. However, the situations can also occur where the interaction has a local minimum at an intermediate length scale. This is expected to be realized in thin films of type-1.5 superconductors, where at long range the interaction should be repulsive due to stray fields [12] and in layered systems where there are different magnetic field penetration lengths in different layers [11,12,21]. Multiple repulsive length scales can also arise as an intrinsic feature in certain anisotropic models [16]. It is worth mentioning that our Hamiltonian and the equations of motion for molecular dynamics (MD) [Eq. (5)] are both dimensionless. The characteristic length scales α_l of attractive and repulsive parts of interaction are set by the coherence lengths and the magnetic field penetration lengths, respectively. The prefactors C_l are set by condensate densities. For a conversion to physical units of Ginzburg-Landau models, please see, e.g., Refs. [5–9,14].

Since we are interested in not very dense ensembles, the only retained attractive Bessel function corresponds to the interactions of larger cores. We consider a bilayer system with different penetration lengths that is approximated by two repulsive Bessel functions. Note that the potential with such an intermediate minimum also arises in a thin film of type-1.5 superconductors where, instead of the Bessel function with the largest length, one includes a power-law repulsion [12]. We emphasize that this does not affect the existence of cluster

crystals, which appear at moderately low densities. Such a regime is the main focus of this paper.

We briefly compare our potential to other commonly used cluster-forming potentials. In addition to Ref. [12], our potential is also similar to ultrasoft potentials such as $U(r) = 1/(1 + r^6)$ [43] in the intermediate and long ranges but differs near the origin. Therefore, the resulting phase diagrams differ at high densities, but all three potentials lead to cluster crystal phases at low densities. Our potential has a characteristic medium attractive range from the attractive Bessel term. This feature is similar to the potential studied in Ref. [27], which is a sum of a repulsive Coulomb term and an attractive exponential term. The two potentials again differ near the origin and therefore the high-density regimes will be different.

B. Observables and methods

Both static and dynamical properties of the system were studied for a large range of particle as well as trap densities using Monte Carlo (MC) and MD simulations. The simulations have three different parts. First, equilibrium sampling was used to map the phase diagram of the clean system with no pinning and no driving, i.e., $U_p = F_D = 0$. The transition temperatures as well as the ordered low-temperature phases were obtained using parallel tempering MC [44–46]. The calculations were complemented by simulated annealing MC [47] as a consistency check. While simulated annealing cannot faithfully maintain thermal equilibrium at low temperatures, it can nevertheless capture the essential features of the phases, e.g., produce typical low energy states [29,43]. We used the Metropolis algorithm with a sequential update order of the particles.

For glass formation simulations with pinning but no driving, i.e., $U_p \neq 0$ and $F_D = 0$, we have used single temperature MC simulations and a random update order of the particles starting from fully disordered configurations.

For the depinning transition, both pinning and driving are included, i.e., $U_p \neq 0$ and $F_D \neq 0$. Since it is unclear if MC can correctly capture transport dynamics, we instead used MD for this paper. Details of the MD simulation of the overdamped Langevin dynamics are discussed in Sec. III B.

The MC simulation methods used here are essentially the same as in Ref. [43]. Each MC sweep for a replica is N attempted updates of the particles in either sequential or random order. The MC trial moves are attempts to shift the particle position randomly within a square box of length $2/\sqrt{n}$ centered on the particle. We only use single-particle update moves. For glass formation dynamics, this corresponds to the overdamped regime.

The main observables are the cluster orientational order parameter ϕ_6 , the heat capacity $C_V = \beta^2 \text{var}(E)$, where E is the total energy of the system, and the pair correlation function $g(r)$. ϕ_6 quantifies the ordering of the triangular cluster-crystal phase. C_V is used for estimating the equilibrium transition temperature for the free case, where it has a prominent peak. $g(r)$ is useful for identifying the presence of particle clustering.

The calculation of ϕ_6 for a given configuration is based on the cluster positions and we now discuss in detail how to compute it. We first use a hierarchical clustering technique

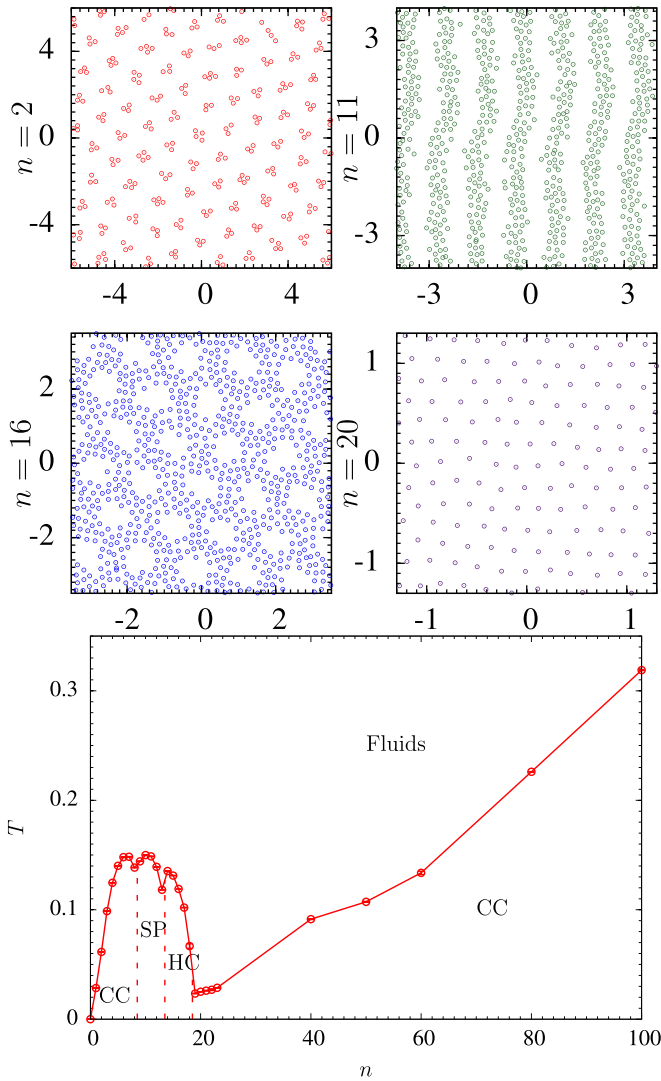


FIG. 2. Top panels: Typical equilibrium configurations of the ordered phases of cluster crystals (CC), stripes (SP), hole crystals (HC) and simple crystals in order of increasing density. Bottom panel: The schematic phase diagram of the potential [Eq. (2)] in absence of pinning disorder estimated from the major peak of the specific heat. The two cluster crystal phases have clustering onset densities at about $n_c = 0.65$ and 30.5 , respectively.

[48,49] that groups particles into clusters deterministically. Each particle starts as a single cluster and the two closest clusters are joined together if their center of mass distance is smaller than a chosen cutoff. We used a cutoff of $0.7 \approx a/2$, where a is the lattice constant of the corresponding cluster crystal in the absence of pinning disorder; see Fig. 2. The results presented in this paper are not sensitive to the precise value of the chosen cutoff, e.g., around 0.7 ± 0.1 , as we work in parameter regimes where clusters are reasonably well-defined. When two clusters are merged, the new center of mass is updated. The process is repeated until no further grouping is accepted. Hence the process takes a particle configuration $\{\vec{r}_i, i = 1, 2, \dots, N\}$ and outputs the centers of mass $\{R_i, i = 1, 2, \dots, C\}$ of the C clusters. The clustering process is

followed by a Voronoi decomposition to identify neighboring clusters.

The orientational order parameter ϕ_6 is finally defined as

$$\phi_6 = \left| \frac{1}{C} \sum_{j=1}^C \left(\frac{1}{N_j} \sum_{\ell=1}^{N_j} e^{i6\theta_{j\ell}} \right) \right|, \quad (3)$$

where $\theta_{j\ell}$ is the angle between the vector $\vec{R}_\ell - \vec{R}_j$ and an arbitrary direction, often the \hat{x} axis, and N_j is the number of neighbors of the j th cluster. Note that only neighboring pairs are summed over. For a perfect triangular lattice, $\phi_6 = 1$, and with no long-range order and random positions, $\phi_6 = 0$. Hence ϕ_6 is an order parameter.

The pair correlation function is defined as

$$g(r) = \frac{1}{N} \frac{\delta n(r)}{2\pi r \delta r}, \quad (4)$$

where $\delta n(r)$ is the number of particles in the shell $2\pi r \delta r$, with reference to an arbitrary particle. Note that the function is normalized as $\int_0^\infty g(r) 2\pi r dr = 1$. The lattice constant of a cluster configuration can be extracted from the peaks of $g(r)$.

III. NUMERICAL RESULTS

A. Cluster glass formation

To study cluster glass formation, it is important to study the underlying pure system without pinning disorder for input, particularly, the relevant particle density for clustering and the corresponding transition temperature. The phase diagram of the pure system along with all the ordered phases are depicted in Fig. 2. Here, the transition temperature is estimated from the prominent C_V peak using $N = 1000$, which is sufficiently large for a reasonably accurate estimation. The linear system size is $L = \sqrt{N/n}$ and at $N = 1000$ it equals, e.g., 22.3607, 9.5346, 7.9057, 7.0711 at $n = 2, 11, 16, 20$, respectively. The crystalline phases are identified by examining typical low-temperature equilibrium configurations and they are also verified from ground states found by simulated annealing. It should be noted that our phase diagram here is only a sketch, and the more subtle features such as the number and the order of these phase transitions are not considered. For the potential in Eq. (2), we find ordered phases of cluster crystals, stripes, and hole crystals as the particle density is increased up to about $n = 18$. This series of ordered phases appears to be rather common in cluster-forming potentials with a repulsive core [12,27]. Note that our potential restores the cluster crystal phase at even higher densities after the hole crystal phase. This behavior is different from the potentials with divergent cores near $r = 0$; cf. Refs. [12,27]. It should be noted that this second cluster phase at high density differs from the first cluster phase at low density with, e.g., a very distinct lattice constant. While pattern formations and the nature of these phase transitions are interesting in their own right, we here focus on the glass formation of the physically relevant low-density cluster phase.

We now present more details of the first triangular cluster phase. The onset density of clustering is at about $n_c = 0.65$, below which there is only one particle per unit cell. When clustering occurs, the lattice constant settles to $a \approx 1.34$, which is estimated from the pair correlation function and is

independent of the density. Interestingly, both the onset density and the lattice constant are very similar to that of the ultrasoft potential $U(r) = 1/(1+r^6)$ [43]. This is presumably because the two potentials have, in some sense, similar features in the medium and long ranges. In the following, we work with a typical cluster phase at density $n = 2$, where each cluster typically has three or four particles. The transition temperature at this density is $\beta_c \approx 16.3$. We now turn to the cluster glass formation of this system.

In the absence of pinning disorder, clustering particles form cluster glasses when quenched from a high temperature, e.g., $T = \infty$ to a sufficiently low temperature in a single step [12]. The system relaxes following the quench, and it was found that the system can reasonably restore the equilibrium order parameter except when the final quenching temperature T_f is too low. The glass transition temperature is then loosely defined when the resulting order parameter ϕ_6 departs from that of the equilibrium cluster crystal phase. It was argued in Ref. [12] that cluster-forming particles are better glass formers compared with non-cluster-forming particles because of the effective polydispersity of the cluster sizes. On the other hand, it is well known that pinning by itself can lead to glass formation in conventional vortex matter [1]. We next investigate the situation where both mechanisms are present.

For the simulation of thermal quench dynamics in the presence of pinning disorder, we consider different density and strength of pinning centers, and compare results with the case of no pinning. For each set of parameters we run quench dynamics to various final temperatures T_f from random configurations corresponding to $\beta = 0$, using single-temperature MC dynamics. For all the temperatures we studied, 10^5 sweeps were enough for a good relaxation, and then the order parameter ϕ_6 of the final configuration was measured. Only one measurement per temperature was made from one disorder realization to prevent correlations, and statistics were collected using averages over disorder realizations. Here, 100 realizations are simulated for each pinning density and strength. We work with particle density $n = 2$ below in this paper unless otherwise specified.

Results for dynamical glass formation are summarized in Fig. 3. In all panels, the red (topmost) curve corresponds to thermal quench of the clean system. This result is similar to that of the MD for other cluster-forming potentials [12]. There are two relevant temperature scales, one is the transition temperature of the pure system where the system forms global order as temperature is lowered below T_c . This matches well with the transition temperature we find from the heat capacity. The other temperature is the crystal-to-glass transition temperature T_G [12], which can be estimated as where ϕ_6 bends downward and starts to drop, here, $T_G \approx 0.05$. This is a characteristic temperature below which dynamics becomes glassy and the system falls out of equilibrium.

It is natural that the clean curve provides an upper bound for restoring the global order, since adding random pinning and increasing the pinning strength generally enhance glass formation. However, it is interesting to note that the effect of pinning is far from linear. Pinning actually has little effect on the order parameter if the disorder is weak or dilute. For example, at $U_p = 1$ there is no prominent change of the order parameter up to about $m = 0.32$. Further increasing the

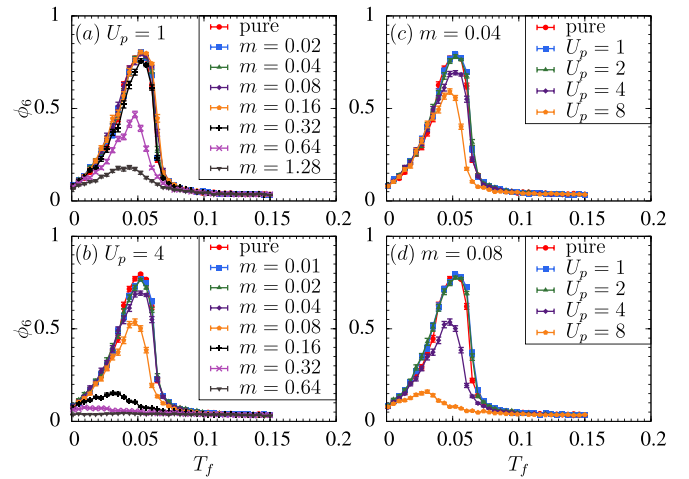


FIG. 3. Effects of density and pinning strength on glass formation after a thermal quench as a function of the final temperature T_f at density $n = 2$ with $N = 1000$ particles. The topmost red curve in each panel is the pure case without disorder, which provides an upper bound. Left panels: Changing the pinning density m at fixed trapping strengths (a) $U_p = 1$ and (b) $U_p = 4$. Right panels: Changing the pinning strength at fixed pinning densities for (c) $m = 0.04$ and (d) $m = 0.08$.

number of pins or the pinning strength eventually makes the order depart prominently from the clean limit. In the strong pinning limit, the global order is essentially entirely eliminated. Another interesting observation that can be drawn from Fig. 3 is that addition of pinning gives the strongest suppression of the ϕ_6 order parameter at intermediate temperatures, while at least for relatively dilute pinning the curves merge with the clean curve at lower temperatures. This suggests that at least for dilute pinning the system falls into a state similar to that of an interaction-dominated effective polydispersity class pinned by rare pinning centers.

It is important to confirm that the quenched glasses are genuine cluster glasses in the presence of substrate disorder. To this end, we have checked the final configurations. Several typical cases are illustrated in the top panels of Fig. 4. The blue circles are Gaussian traps. It is clear from observation that clusters are still reasonably well-defined despite the attractive traps distorting the cluster order as well as the distribution of cluster sizes. For example, it is more likely to find larger clusters in or near the (overlapping) traps. Interestingly, these clusters do not necessarily all sit at the trap centers. In the dense case $m = 1.28$, there are a number of large clusters of sizes 5, 6, and even 7, leaving at the same time some small clusters in the trap interstitial voids.

Cluster glass manifests itself when the corresponding cluster crystal lattice constant peak is relevant in the pair correlation function. This is shown in the bottom panel of Fig. 4 for various m values. It is seen that the second largest peak, which is the cluster crystal lattice constant peak, is present for all cases studied. The peak near $r = 0$ is from the neighboring particles within clusters. Note that a small shoulder peak is developed for the dense cases $m = 0.64$ and 1.28 , as some clusters are larger compared with the typical size of

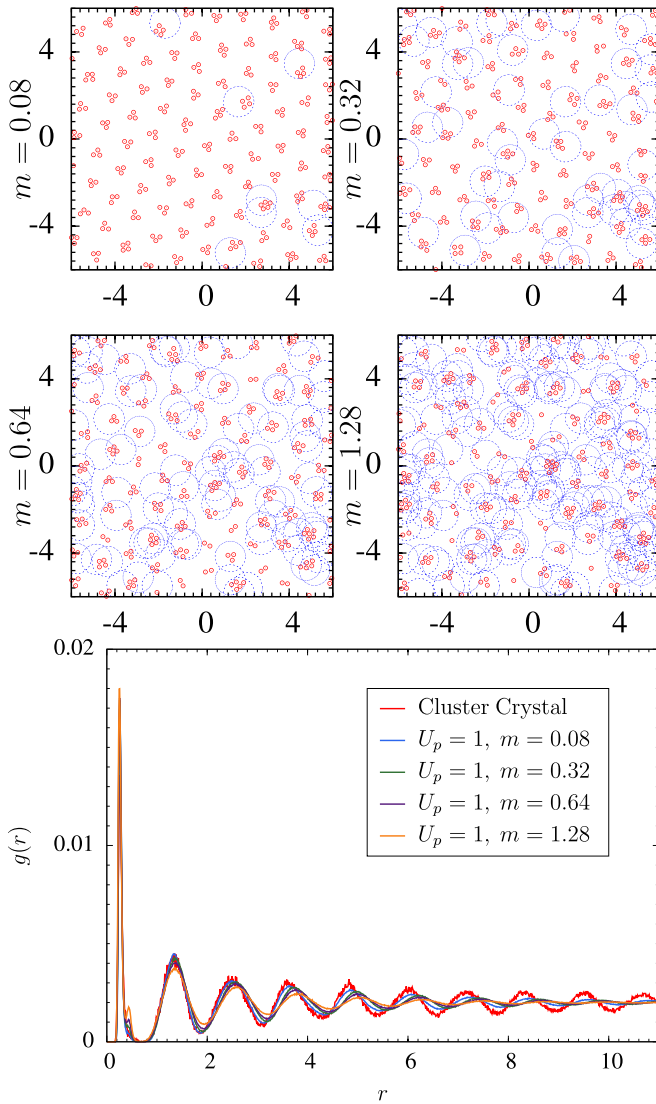


FIG. 4. Top panels: Typical cluster glass configurations corresponding to those of Fig. 3 at approximately $T = 0.03$, the particle density is $n = 2$. The blue dashed circles are attractive Gaussian centers. Note that a fraction of some large clusters is formed in or near the (overlapping) traps. These configurations suggest that clusters are reasonably well-defined in our parameter regimes. Bottom panel: The clustering feature is further confirmed in the pair correlation function $g(r)$. Particularly, the second largest peak is the intercluster peak, or the lattice constant peak of the corresponding cluster crystal.

the free case. By contrast, the lattice constant of the particle triangular crystal $3^{-1/4} = 0.7598$ at the same density is not relevant.

It is important to note that we should not take the weak and strong traps here too literally, as in our cases cluster glasses are *all* reasonably well-defined. It is clearly possible to further increase the trap depth, and new phases, e.g., particle glasses may appear. It is expected that fully formed particle glasses should emerge in certain trap settings, depending on the trap size, depth, and density. The main conclusion of this section is that interaction-driven cluster glasses are stable with respect to inclusion of quenched disorder in the parameter regime studied here.

B. Cluster glass depinning dynamics

In this section, we use MD to study the depinning dynamics of the cluster glasses we obtained. We use the overdamped Langevin dynamics given by

$$\gamma \dot{\vec{r}}_i = -\nabla U_i + \sqrt{2T\gamma} \vec{\eta}_i(t) + F_D \hat{x}, \quad (5)$$

where, without loss of generality, we set the friction coefficient $\gamma = 1$. The Gaussian stochastic force η has zero mean and is uncorrelated in time, $\langle \eta_{i\alpha}(t) \eta_{i\gamma}(t') \rangle = \delta(t-t') \delta_{\alpha\gamma}$, where $\alpha, \gamma = x, y$ denote components in different spatial directions. U_i is the potential energy of particle i interacting with other particles and the traps, and F_D is applied along the \hat{x} axis. For the thermal noise in each direction, it is straightforward to show from the correlation function that $\int_t^{t+dt} \sqrt{2T} \eta_{i\alpha}(t') dt' = \sqrt{2T dt} \zeta$, where ζ follows the standard Gaussian distribution $n(0, 1)$. In the large driving limit, we expect a drift velocity $v = \langle v_x \rangle = F_D$ as in the case of single particles [28]. The force on a particle for the symmetric potential is given by $F(r) = -\hat{r} dV/dr$, where $-dK_0(r)/dr = K_1(r)$ is the modified Bessel function of the second kind. K_1 is similar in shape to K_0 but it is further shifted away from $r = 0$. The integration is done using the fourth-order Runge-Kutta method. We investigate the cluster glass depinning for a typical case of $U_p = 1$ at $T = T_C/2$, where various features of the cluster flow can be studied. In certain cases, we also performed simulations at $T = 0$ to suppress thermal fluctuations to get a clear visualization of the dynamics.

In the pure case with no pinning, the clusters slide together along the direction of the driving force, and the drift velocity is given by the linear relation $v = F_D$ for any F_D ; see the (top-most) red line of Fig. 5. At finite temperatures, the particles will fluctuate while sliding but the underlying cluster glass order is unchanged. When the temperature is quenched to $T = 0$, the internal dynamics of the clusters will be rapidly frozen and the cluster glass essentially slides rigidly afterward. In either case, the cluster glass remains intact. These observations are expected since, without pinning, the particle motion is given by a superposition of the internal dynamics when driving is absent and a constant translation motion, i.e., in the absence of pinning, the state can be simply identified as a *sliding cluster glass*. A typical movie of such dynamics for $F_D = 0.2$ at both finite and zero temperatures is presented in Ref. [50].

In the presence of pinning, a dynamical depinning transition should occur as the driving force is increased. We performed large-scale MD simulations to measure the disorder-averaged drift velocity at various driving forces. For each run, we integrate up to a sufficiently long time $t = 1000$, and the drift velocity is measured using the latter half of the simulation, i.e., the initial transient dynamics is ignored and we measure the asymptotic steady state drift velocity. The results are shown in Fig. 5. For moderate and dense pinning, there is a prominent pinned phase. The critical depinning force is naturally very small but nonzero when the pinning is dilute. Detailed examination near $F_D = 0$ reveals that there are pinned phases as well for dilute pinning. Fisher showed that a pinned to sliding transition can have features similar to critical phenomena with a power-law dependence of the nonlinear velocity-force characteristic of the form $v \sim (F_D - F_C)^\beta$ for

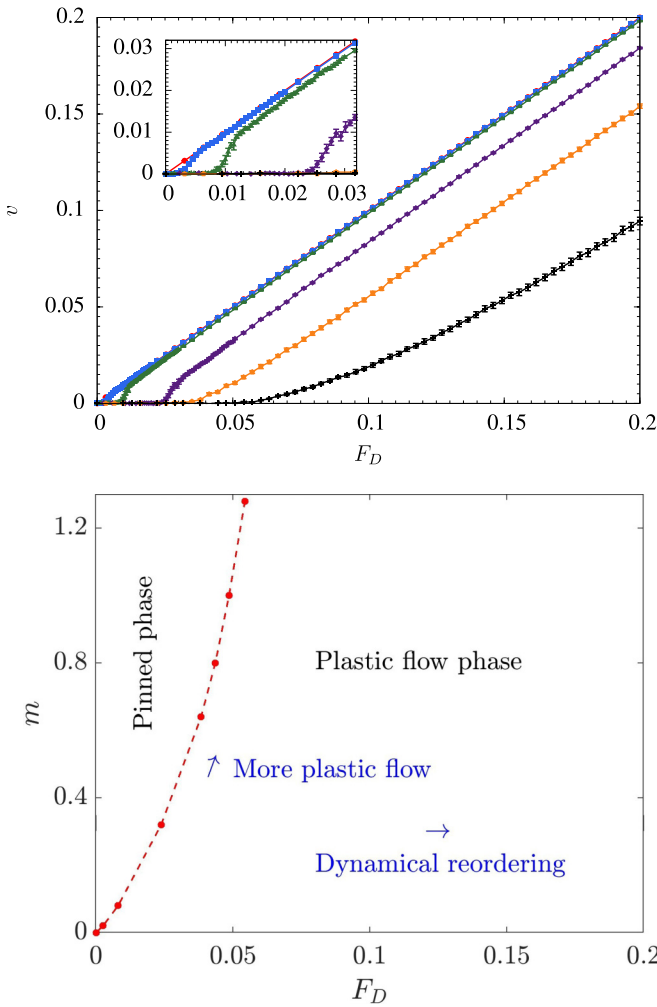


FIG. 5. Top: Drift velocity as a function of the external driving force at $T = T_C/2$ for, from left to right, the pure system, $m = 0.02, 0.08, 0.32, 0.64,$ and 1.28 , respectively. The particle density is again at $n = 2$. The inset panel is a zoom of the main panel near the origin. For the pure case, there is a linear force-velocity relation. For dense pinning, there is a prominent depinning transition and the drift velocity converges slowly to the free case. For dilute pinning, the critical force is much smaller and the drift velocity converges rapidly to the pure case. The concave down form of the depinning curves near the transition suggests plastic depinning, which is confirmed in the flowing dynamics. Bottom: A schematic dynamical phase diagram in the m - F_D parameter space; see the text for the plastic flow features and the corresponding dynamical reordering at large forces.

$F_D \geq F_C$ in the vicinity of the critical depinning force F_C [51]. As the curves in Fig. 5 are concave down near the transition, it suggests that $\beta > 1$, i.e., the depinning is likely plastic [28]. In plastic flows, particles or clusters change their neighbors during the flow, contrary to the elastic flow where neighboring particles and clusters are preserved. A close examination of the dynamics shows that the cluster flows are indeed plastic, with a number of features distinct from the non-cluster-forming particle systems, e.g., clusters undergo merging and breaking dynamics.

We discuss the dense pinning first, where the flowing phase is clearly plastic. The flowing dynamics is quite complex, and

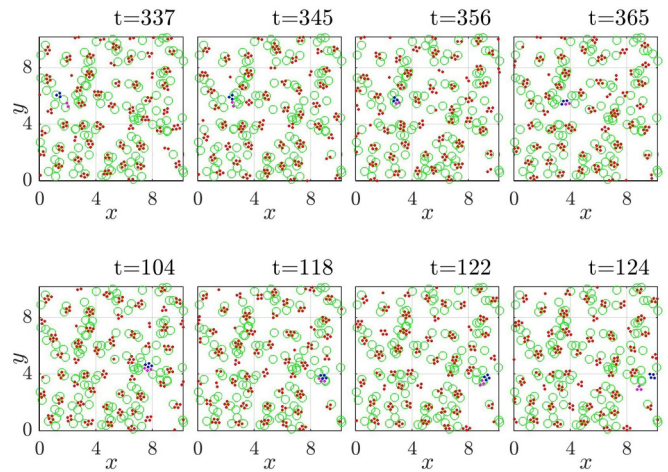


FIG. 6. Typical clusters merging (top panels) and splitting (bottom panels) dynamics induced by the trap centers ($T = 0$), the pertinent clusters are in blue and pink while other clusters are in red, and the green circles are pinning centers. In this dense pinning regime, such processes are frequent, rendering the flow highly plastic.

here we focus on the main features and typical dynamical processes. Considering the complexity of the flow, a movie showing both the pinned and flowing phases is shown in Ref. [52], where the driving forces are $F_D = 0.0508$ and 0.2 , respectively, for a disorder realization of $m = 1.28$. There are a number of interesting observations for the flowing phase. First, chaotic cluster flow occurs instead of the chaotic particle flow in non-cluster-forming ensembles. Here, the clusters have a strong tendency to flow through or near the traps, forming rivers and changing neighbors. Interestingly, the pinning centers are like stepping stones for the clusters. In addition, the clusters are no longer as robust as in the free case. There are frequent clusters merging and breaking dynamics. For example, unusually large clusters may form as a result of merging and there are also a number of single-particle clusters as a result of particle emission from clusters. As a result, the clusters are much more heterogeneous than the pure case due to the interplay of pinning and driving. It is important to emphasize that this increased heterogeneity is *not* a result of thermal noise as we are working in the low-temperature glass phase, despite that it also contributes. This is clearly demonstrated as the above processes also occur at $T = 0$ as shown in the movie in Ref. [53]. A typical cluster merging process and also a cluster splitting process are depicted in Fig. 6. It is interesting that trap centers play a catalytic role for the dynamics. Indeed, the plastic processes are much suppressed in the dilute pinning regime.

In the opposite dilute pinning regime, the flow is much more ordered. After close inspections of $m = 0.02$, we find that the flow is still plastic, but the plastic processes are relatively rare. Upon depinning, the glass mostly slides over the pinning centers. The plastic flow and cluster merging and breaking processes are much suppressed. Nevertheless, the effective polydispersity of the clusters can still enable trap-induced neighbor-changing dynamics because of their different mobilities. Similar to a cluster liquid [43], small

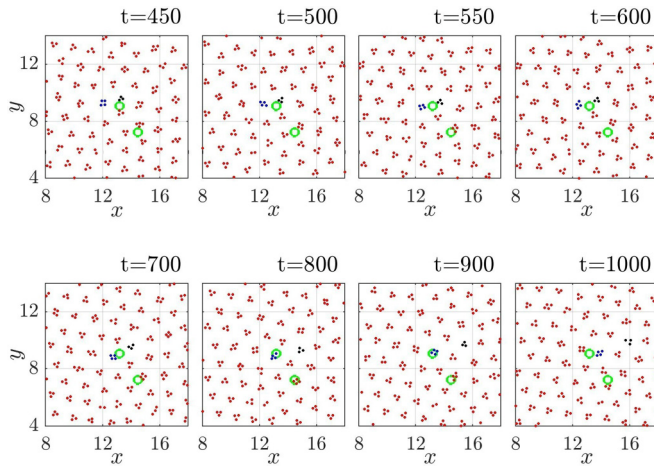


FIG. 7. Example of a plastic neighbor-changing process for a dilute pinning case with $m = 0.02$. The clusters can change their neighbors due to their polydispersity and, consequently, their mobilities. Here, the smaller black cluster depins faster and has a better mobility. As a result, when the blue cluster depins, the black cluster is no longer a neighbor of the blue cluster, inducing weak plastic flows.

clusters tend to have better mobilities and, moreover, larger clusters are better pinned by impurity traps.

Figure 7 illustrates a neighbor-changing plastic flow process in the dilute pinning case. Here, the two relevant clusters are highlighted in blue and black. The blue cluster has four particles while the black cluster has three particles. The black cluster depins at around $t = 450$ and afterward the blue cluster arrives at the pinning center and is temporarily pinned. This pinning is stronger than that of the black one as there are more particles, and also, importantly, a smaller cluster has a higher mobility and is easier to diffuse around. As a result, although the blue cluster eventually also depins at around $t = 1000$, the black cluster has already diffused away and is thus no longer a neighbor of the blue cluster. This process makes the flow weakly plastic. However, such events do not occur frequently for dilute pinning compared to the time scale of the data in Fig. 6.

While the vortex-glass depinning may appear to be similar to the vortex-glass melting [1,32,40,41], we should note a major difference in the present clustering case: upon heating, a cluster glass relaxes to a well-ordered cluster crystal instead of melting to a disordered state. The mechanism is described in Ref. [25] and is based on the thermal activation of the hopping of individual vortices over the whole clusters structure. This removes the polydispersity and, consequently, the uneven bond connectivity of the clusters with increasing temperature within the solid phase.

To summarize this section, all the depinning flows that we studied are plastic cluster flows. Clusters tend to flow along pinning channels when pinning is dense. The effective polydispersity assists plastic flows in two aspects. First, it generates new forms of plastic flow processes such as clusters merging and breaking. In addition, their different mobilities can also induce neighbor-changing plastic flows when flowing through the pinning centers. These are quite distinct features from the depinning of ordinary non-cluster-forming glasses.

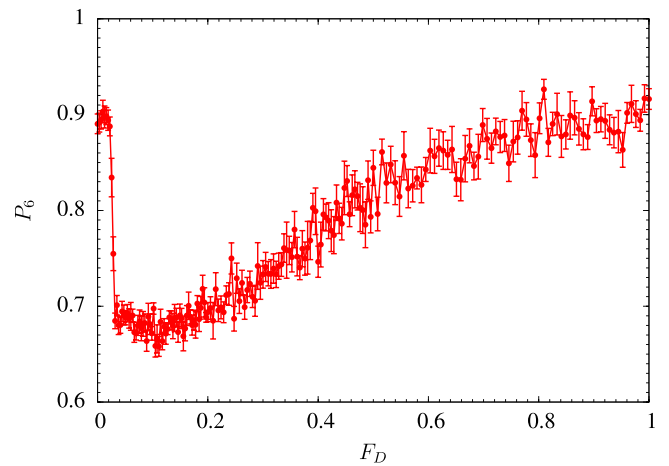


FIG. 8. Cluster glass plastic flow exhibits dynamical reordering when the driving force is increased. Here the fraction P_6 of clusters with six neighboring clusters is shown as a function of the driving force for $m = 0.32$. The fraction decreases significantly at the onset of the plastic flow around $F_D = 0.02$, but it then gradually restores when F_D is increased as the pinning effects are increasingly washed out. Note that this dynamical reordering appears to be a crossover rather than a genuine phase transition. Here, the pinning strength is $U_p = 1$ and the particle density is $n = 2$.

A schematic dynamical phase diagram is summarized in the bottom of Fig. 5, and we now turn to the dynamical reordering as the force increases.

C. Dynamical reordering, critical exponent, and comparison with particle glass

In this section, we first demonstrate that cluster glasses upon depinning can undergo dynamical reordering when the driving force is increased. Next, we measure the critical exponent β of the depinning transition. Finally, the cluster glass pinning strength is compared with that of ordinary particle glass, finding that cluster glass can have much stronger pinning effects than particle glass. This is potentially useful in superconductor applications.

It is well known that the particle glass and the stripe pattern-forming systems can exhibit dynamical reordering as the driving force is increased [26,28]. For example, stripes may break into pieces in presence of pinning disorder but, upon depinning, stripes may reform when the driving force gets larger. Here, we investigate this phenomenon for the cluster glass. To study the dynamical reordering, we look at an order statistic P_6 . This is the fraction of clusters having six cluster neighbors in the asymptotic steady state as a function of the driving force. The result of $m = 0.32$ is shown in Fig. 8. It is interesting that P_6 drops very sharply at the onset of the plastic flow, the critical force here is in good agreement with the depinning transition of Fig. 5. This indicates that the system in the flowing phase is most chaotic when it just depins, and pinning and driving compete most strongly near the depinning transition. As the driving force increases, it is remarkable that P_6 is gradually restored and the effects of pinning are increasingly washed out; note that the force scale is larger than that of Fig. 5. When $F_D \gtrsim 0.8$, P_6 is almost the

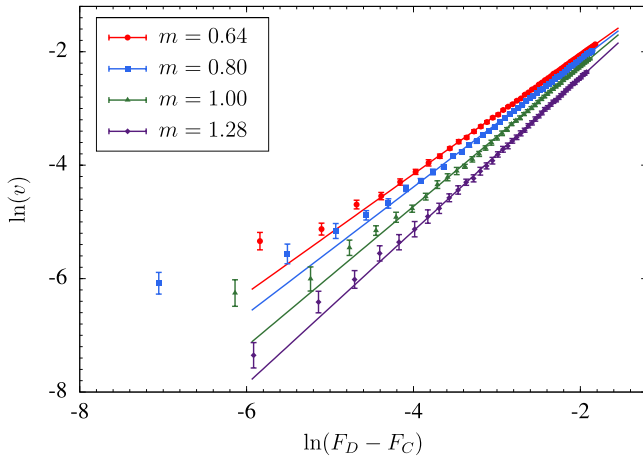


FIG. 9. Power-law scaling of the velocity v versus $F_D - F_C$ near the transition for $m = 0.64, 0.80, 1.00$, and 1.28 . While the power-law behavior appears to be reasonably good in all cases, the exponent or the slope becomes slightly larger with the increasing number of pinning centers, yielding $\beta = 1.049(5), 1.121(5), 1.233(8)$, and $1.351(13)$, respectively. See the text for more discussions. Here, the pinning strength is $U_p = 1$ and the particle density is $n = 2$.

same as that of the pinned phase. However, it seems that the reordering is by no means perfect; it does not achieve a perfect order for the largest force we studied, which is approximately 50 times larger than the depinning force. In addition, the reordering occurs gradually and appears to be a crossover rather than a genuine phase transition.

We next study the force-velocity relation at the depinning transition. We define a critical exponent as $v \sim (F_D - F_C)^\beta$ for $F_D \geq F_C$ in the vicinity of the depinning threshold force F_C . When the pinning is dilute, the range of F_D where a power-law behavior applies is limited; see Fig. 5. By contrast, the depinning in the dense pinning regime has a much wider range of forces pertinent to power-law scaling, and we therefore compute β using the cases $m = 0.64$ and 1.28 . We use a cubic function fit in the flowing phase but keep away from the transition to first locate the critical force F_C and then make a power-law fit. In both cases, we find good power-law behaviors and the scaling plots are shown in Fig. 9. The two exponents are close but slightly different, $\beta = 1.049(5)$ and $1.351(13)$, respectively. Adding two intermediate cases $m = 0.80$ and 1.00 , we find that there appears to be a slow drift of the exponent β .

This exponent is, unfortunately, in general very poorly understood, and it is yet unclear whether there is a universality class for plastic depinning. Our case appears to be even more complicated as our starting configurations are by design quenched glasses rather than slowly annealed states. Hence, it is not clear whether different pinning densities, corresponding to different degrees of glassiness, necessarily have the same critical exponent. More pinning centers introduce more defects into the quenched cluster glass, and therefore the depinning could be more plastic for a denser pinning, yielding a slightly larger critical exponent. On the other hand, our computed exponents also fall within the broad range of exponents found for plastic depinning in many different systems [28]. Therefore, this could be a finite-size effect or

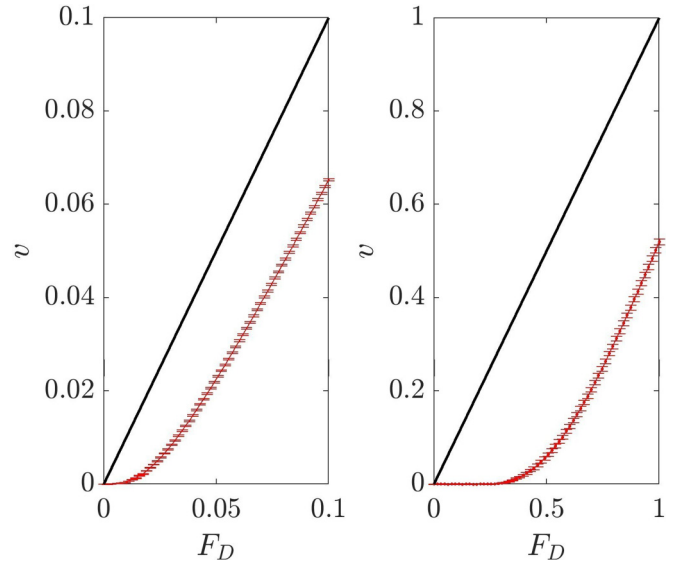


FIG. 10. Velocity-force curve for particle glass (left) and cluster glass (right) for $m = 0.64$ and $U_p = 1$. The trap size is $\sigma = 0.3799$, which is half the lattice constant of the particle crystal. Both glass formation and molecular dynamics are performed at their respective $T_C/2$. Note that the depinning force of the cluster glass is much larger than that of the particle glass, suggesting vortex clusters can have much better pinning properties than ordinary single vortices.

finite-temperature effect and there is a universality class or, alternatively, quenched glasses may be different from annealed glasses. This intriguing question requires further systematic studies and will not be discussed more here.

Finally, we compare the depinning forces of cluster glasses and particle glasses. To this end, we have simulated $N = 1000$ particles at density $n = 2$, interacting with a single Bessel function potential as shown in Fig. 1. The numerical setup is essentially the same for particle glasses, except that the temperature scales differ. Here, the transition temperature of the pure system is much smaller, $T_C \approx 0.01077$. Similarly, we prepare glasses and do MD in the presence of pinning at its own $T_C/2$.

We consider the pinning density $m = 0.64$ and $N = 1000$ particles. We have similarly checked that the quenched states are particle glasses with $\phi_6 \lesssim 0.1$. There are two natural choices of the trap size σ for a fair comparison, i.e., we can use either half the lattice constant of the cluster crystal or the particle crystal. For the same trap depth $U_p = 1$, they yield wider or narrower traps, or weaker or stronger pinning, respectively. Fortunately, they yield qualitatively the same conclusion. When wider traps are used, the particle glass has a very small depinning force that is not easily measurable, i.e., the traps are too wide to pin the particle glass effectively. Hence we use smaller traps for *both* systems and the results are shown in Fig. 10. It is found that the cluster glass again pins much better than the particle glass; the critical forces are approximately $F_C = 0.01$ for particle glass and 0.3 for cluster glass. There are many parameters including the interaction potentials that one can tune to explore this more systematically. However, considering that the depinning force scales are very different in the cases studied here, it is quite suggestive

that cluster-forming type-1.5 superconductors can have much better pinning properties than systems of ordinary vortices.

IV. CONCLUSIONS

We studied an ensemble of two-dimensional monodisperse particles interacting via a cluster-forming potential, relevant to vortices in type-1.5 superconductors in the presence of demagnetizing fields and layered type-1.5 systems. Vortices in such systems were previously demonstrated to form glasses in the absence of pinning, purely due to peculiarities of inter-vortex forces. Similar potentials also arise in quantum Hall physics [34,35] and soft matter.

We examined cluster glass formation following a thermal quench in the presence of pinning centers of moderate depth and the corresponding depinning transition. We find that weak and dilute pinning have little effects on the interaction-dominated glass formation: the disordered configuration adapts to the presence of dilute pinning sites, preserving the intervortex-interaction-driven effective polydispersity.

However, moderate, strong, and dense pinning can substantially assist glass formation, especially at intermediate temperatures, and indeed can entirely remove order. For the pinning strength we have studied, the depinning transition is plastic and the cluster plastic flow exhibits features distinct from particle plastic flow. This includes cluster chaotic flow, clusters merging and breaking, and their different mobilities. Therefore, the effective polydispersity of clusters assists both glass formation and plastic flows. The cluster plastic flow is also found to exhibit dynamical reordering when the driving force is large.

Finally, a conclusion of practical importance is that cluster glasses can have significantly better pinning properties than systems of non-cluster-forming particles. Since vortex pinning is important for transport properties of superconductors,

it suggests that these properties of type-1.5 superconductors can be useful in applications. Cluster-forming potentials can be engineered, for example, by layering systems [21] or by using superconductors where there is an additional phase transition associated with the time-reversal symmetry breakdown [13,14].

Future work should characterize the cluster plastic flow at a quantitative level. This is a challenging task compared with particle plastic flow because the clusters are constantly merging and breaking like in a cluster liquid [43], at least when the plastic flow is (reasonably) strong. Effective criteria and statistics should be defined, e.g., to extract the cluster size and lifetime distributions for a given flowing dynamics. In addition, it is worthwhile to optimize the cluster-forming potential to further improve the pinning properties. Research work along these lines is currently in progress and will be reported in future publications.

ACKNOWLEDGMENTS

We thank Cynthia Reichhardt for helpful exchanges on depinning transitions and Alexander Zyuzin for helpful discussions. W.W. and E.B. acknowledge support from the Göran Gustafsson Foundation for Research in Natural Sciences and Medicine. E.B. acknowledges support from Swedish Research Council Grants No. 642-2013-7837, No. 2016-06122, No. 2018-03659, and the Olle Engkvists Stiftelse. W.W. also acknowledges support from the Fundamental Research Funds for the Central Universities, China. The computations were performed on resources provided by the Swedish National Infrastructure for Computing (SNIC) at the National Supercomputer Center in Linköping, Sweden, and the High Performance Computing Center North (HPC2N) partially funded by the Swedish Research Council through Grant Agreement No. 2018-05973.

-
- [1] G. Blatter, M. V. Feigelman, V. B. Geshkenbein, A. I. Larkin, and V. M. Vinokur, Vortices in high-temperature superconductors, *Rev. Mod. Phys.* **66**, 1125 (1994).
 - [2] M. P. A. Fisher, Vortex-Glass Superconductivity: A Possible New Phase in Bulk High- T_c oxides, *Phys. Rev. Lett.* **62**, 1415 (1989).
 - [3] D. S. Fisher, M. P. A. Fisher, and D. A. Huse, Thermal fluctuations, quenched disorder, phase transitions, and transport in type-II superconductors, *Phys. Rev. B* **43**, 130 (1991).
 - [4] D. R. Nelson, *Defects and Geometry in Condensed Matter Physics* (Cambridge University Press, Cambridge, 2002).
 - [5] E. Babaev and M. Speight, Semi-Meissner state and neither type-I nor type-II superconductivity in multicomponent superconductors, *Phys. Rev. B* **72**, 180502(R) (2005).
 - [6] E. Babaev, J. Carlström, and M. Speight, Type-1.5 Superconducting State from an Intrinsic Proximity Effect in Two-Band Superconductors, *Phys. Rev. Lett.* **105**, 067003 (2010).
 - [7] J. Carlström, E. Babaev, and M. Speight, Type-1.5 superconductivity in multiband systems: Effects of interband couplings, *Phys. Rev. B* **83**, 174509 (2011).
 - [8] M. Silaev and E. Babaev, Microscopic theory of type-1.5 superconductivity in multiband systems, *Phys. Rev. B* **84**, 094515 (2011).
 - [9] E. Babaev, J. Carlström, M. Silaev, and J. Speight, Type-1.5 superconductivity in multicomponent systems, *Physica C: Superconductivity and its applications* **533**, 20 (2017).
 - [10] J. Carlström, J. Garaud, and E. Babaev, Semi-Meissner state and nonpairwise intervortex interactions in type-1.5 superconductors, *Phys. Rev. B* **84**, 134515 (2011).
 - [11] C. N. Varney, K. A. Sellin, Q.-Z. Wang, H. Fangohr, and E. Babaev, Hierarchical structure formation in layered superconducting systems with multi-scale inter-vortex interactions, *J. Phys.: Condens. Matter* **25**, 415702 (2013).
 - [12] R. Díaz-Méndez, F. Mezzacapo, W. Lechner, F. Cinti, E. Babaev, and G. Pupillo, Glass Transitions in Monodisperse Cluster-Forming Ensembles: Vortex Matter in Type-1.5 Superconductors, *Phys. Rev. Lett.* **118**, 067001 (2017).

- [13] J. Carlström, J. Garaud, and E. Babaev, Length scales, collective modes, and type-1.5 regimes in three-band superconductors, *Phys. Rev. B* **84**, 134518 (2011).
- [14] J. Garaud, A. Corticelli, M. Silaev, and E. Babaev, Properties of dirty two-band superconductors with repulsive interband interaction: Normal modes, length scales, vortices, and magnetic response, *Phys. Rev. B* **98**, 014520 (2018).
- [15] M. Silaev, T. Winyard, and E. Babaev, Non-London electrodynamics in a multiband London model: Anisotropy-induced nonlocalities and multiple magnetic field penetration lengths, *Phys. Rev. B* **97**, 174504 (2018).
- [16] T. Winyard, M. Silaev, and E. Babaev, Hierarchies of length-scale based typology in anisotropic U(1) *s*-wave multiband superconductors, *Phys. Rev. B* **99**, 064509 (2019).
- [17] J. Pearl, Current distribution in superconducting films carrying quantized fluxoids, *Appl. Phys. Lett.* **5**, 65 (1964).
- [18] V. Moshchalkov, M. Menghini, T. Nishio, Q. H. Chen, A. V. Silhanek, V. H. Dao, L. F. Chibotaru, N. D. Zhigadlo, and J. Karpinski, Type-1.5 superconductivity, *Phys. Rev. Lett.* **102**, 117001 (2009).
- [19] S. J. Ray, A. S. Gibbs, S. J. Bending, P. J. Curran, E. Babaev, C. Baines, A. P. Mackenzie, and S. L. Lee, Muon-spin rotation measurements of the vortex state in Sr_2RuO_4 : Type-1.5 superconductivity, vortex clustering, and a crossover from a triangular to a square vortex lattice, *Phys. Rev. B* **89**, 094504 (2014).
- [20] P. K. Biswas, F. N. Rybakov, R. P. Singh, S. Mukherjee, N. Parzyk, G. Balakrishnan, M. R. Lees, C. D. Dewhurst, E. Babaev, A. D. Hillier, and D. M. K. Paul, Coexistence of type-I and type-II superconductivity signatures in ZrB_{12} probed by muon spin rotation measurements, *Phys. Rev. B* **102**, 144523 (2020).
- [21] Q. Meng, C. N. Varney, H. Fangohr, and E. Babaev, Phase diagrams of vortex matter with multi-scale inter-vortex interactions in layered superconductors, *J. Phys.: Condens. Matter* **29**, 035602 (2016).
- [22] Q. Meng, C. N. Varney, H. Fangohr, and E. Babaev, Honeycomb, square, and kagome vortex lattices in superconducting systems with multiscale intervortex interactions, *Phys. Rev. B* **90**, 020509(R) (2014).
- [23] G. Malescio and G. Pellicane, Stripe phases from isotropic repulsive interactions, *Nat. Mater.* **2**, 97 (2003).
- [24] F. Cinti, T. Macrì, W. Lechner, G. Pupillo, and T. Pohl, Defect-induced supersolidity with soft-core bosons, *Nat. Commun.* **5**, 3235 (2014).
- [25] R. Díaz-Méndez, G. Pupillo, F. Mezzacapo, M. Wallin, J. Lidmar, and E. Babaev, Phase-change switching in 2D via soft interactions, *Soft Matter* **15**, 355 (2019).
- [26] C. Reichhardt, C. J. Olson Reichhardt, I. Martin, and A. R. Bishop, Dynamical Ordering of Driven Stripe Phases in Quenched Disorder, *Phys. Rev. Lett.* **90**, 026401 (2003).
- [27] C. J. Olson Reichhardt, C. Reichhardt, and A. R. Bishop, Structural transitions, melting, and intermediate phases for stripe- and clump-forming systems, *Phys. Rev. E* **82**, 041502 (2010).
- [28] C. Reichhardt and C. J. O. Reichhardt, Depinning and nonequilibrium dynamic phases of particle assemblies driven over random and ordered substrates: A review, *Rep. Prog. Phys.* **80**, 026501 (2016).
- [29] W. L. Miller and A. Cacciuto, Two-dimensional packing of soft particles and the soft generalized Thomson problem, *Soft Matter* **7**, 7552 (2011).
- [30] L. Caprini, E. Hernández-García, and C. López, Cluster crystals with combined soft- and hard-core repulsive interactions, *Phys. Rev. E* **98**, 052607 (2018).
- [31] M. A. Glaser, G. M. Grason, R. D. Kamien, A. Košmrlj, C. D. Santangelo, and P. Zihlerl, Soft spheres make more mesophases, *Europhys. Lett.* **78**, 46004 (2007).
- [32] A. Zaccone, H. Wu, and E. Del Gado, Elasticity of Arrested Short-Ranged Attractive Colloids: Homogeneous and Heterogeneous Glasses, *Phys. Rev. Lett.* **103**, 208301 (2009).
- [33] P. Yunker, Z. Zhang, and A. G. Yodh, Observation of the Disorder-Induced Crystal-to-Glass Transition, *Phys. Rev. Lett.* **104**, 015701 (2010).
- [34] A. A. Koulakov, M. M. Fogler, and B. I. Shklovskii, Charge Density Wave in Two-Dimensional Electron Liquid in Weak Magnetic Field, *Phys. Rev. Lett.* **76**, 499 (1996).
- [35] M. M. Fogler, A. A. Koulakov, and B. I. Shklovskii, Ground state of a two-dimensional electron liquid in a weak magnetic field, *Phys. Rev. B* **54**, 1853 (1996).
- [36] M. Sammon, X. Fu, Y. Huang, M. A. Zudov, B. I. Shklovskii, G. C. Gardner, J. D. Watson, M. J. Manfra, K. W. Baldwin, L. N. Pfeiffer *et al.*, Resistivity anisotropy of quantum Hall stripe phases, *Phys. Rev. B* **100**, 241303(R) (2019).
- [37] Y. Huang, M. Sammon, M. A. Zudov, and B. I. Shklovskii, Isotropically conducting (hidden) quantum Hall stripe phases in a two-dimensional electron gas, *Phys. Rev. B* **101**, 161302(R) (2020).
- [38] M. M. Fogler, Stripe and bubble phases in quantum Hall systems, in *High Magnetic Fields* (Springer, Berlin, 2002), pp. 98–138.
- [39] B. O. Conchúir and A. Zaccone, Mechanism of flow-induced biomolecular and colloidal aggregate breakup, *Phys. Rev. E* **87**, 032310 (2013).
- [40] A. Zaccone and E. Scossa-Romano, Approximate analytical description of the nonaffine response of amorphous solids, *Phys. Rev. B* **83**, 184205 (2011).
- [41] A. Zaccone and E. M. Terentjev, Disorder-Assisted Melting and the Glass Transition in Amorphous Solids, *Phys. Rev. Lett.* **110**, 178002 (2013).
- [42] C. Reichhardt, C. J. O. Reichhardt, and A. R. Bishop, Hysteresis and noise in stripe- and clump-forming systems, *Europhys. Lett.* **72**, 444 (2005).
- [43] W. Wang, R. Díaz-Méndez, M. Wallin, J. Lidmar, and E. Babaev, Melting of a two-dimensional monodisperse cluster crystal to a cluster liquid, *Phys. Rev. E* **99**, 042140 (2019).
- [44] R. H. Swendsen and J.-S. Wang, Replica Monte Carlo Simulations of Spin Glasses, *Phys. Rev. Lett.* **57**, 2607 (1986).
- [45] C. Geyer, in *Computing Science and Statistics: 23rd Symposium on the Interface*, edited by E. M. Keramidas (Interface Foundation, Fairfax Station, 1991), p. 156.
- [46] K. Hukushima and K. Nemoto, Exchange Monte Carlo method and application to spin glass simulations, *J. Phys. Soc. Jpn.* **65**, 1604 (1996).
- [47] S. Kirkpatrick, C. D. Gelatt, and M. P. Vecchi, Optimization by simulated annealing, *Science* **220**, 671 (1983).
- [48] P. Tan, M. Steinbach, and V. Kumar, *Introduction to Data Mining* (Addison-Wesley Longman Publishing Co., Inc., Reading, 2006).

- [49] R. Díaz-Méndez, F. Mezzacapo, F. Cinti, W. Lechner, and G. Pupillo, Monodisperse cluster crystals: Classical and quantum dynamics, *Phys. Rev. E* **92**, 052307 (2015).
- [50] Please see the movie for details: https://www.youtube.com/watch?v=p2_o_eIOpNY.
- [51] D. S. Fisher, Sliding charge-density waves as a dynamic critical phenomenon, *Phys. Rev. B* **31**, 1396 (1985).
- [52] Please see the movie for details: <https://www.youtube.com/watch?v=FtGK1HByCxc>.
- [53] Please see the movie for details: https://www.youtube.com/watch?v=HUxpUV_UNzM&feature=youtu.be.